Eurasian river spring flood observations support net Arctic Ocean mercury export to the atmosphere and Atlantic Ocean

Jeroen E. Sonke[a,1], Roman Teisserenc[b], Lars-Eric Heimbürger-Boavida[a,c], Mariia V. Petrova[c], Nicolas Marusczak[a], Theo Le Dantec[b], Artem V. Chupakov[d], Chuxian Li[a], Colin P. Thackray[e], Elsie M. Sunderland[e], Nikita Tananaev[b,f], and Oleg S. Pokrovsky[a,g]

[a]Laboratoire Géosciences Environnement Toulouse, CNRS/Institute for Research and Development/Université Paul Sabatier–Toulouse III, 31400 Toulouse, France; [b]EcoLab, Université de Toulouse, CNRS, National Polytechnic Institute, 31400 Toulouse, France; [c]Mediterranean Institute of Oceanography, CNRS, Université de Toulon, Institute for Research and Development, Aix-Marseille Université, 13288 Marseille, France; [d]N. Laverov Federal Center for Integrated Arctic Research, Russian Academy of Sciences, 163000 Arkhangelsk, Russia; [e]Environmental Science and Engineering Program, Harvard John A. Paulson School of Engineering and Applied Sciences, Harvard University, Cambridge, MA 02138; [f]Permafrost Groundwater and Geochemistry Laboratory, Melnikov Permafrost Institute, Siberian Branch, Russian Academy of Sciences, 677010 Yakutsk, Russia; and [g]BIO-GEO-CLIM Laboratory, Tomsk State University, 634050 Tomsk, Russia

Edited by Mark H. Thiemens, University of California, San Diego, La Jolla, CA, and approved October 19, 2018 (received for review July 11, 2018)

Midlatitude anthropogenic mercury (Hg) emissions and discharge reach the Arctic Ocean (AO) by atmospheric and oceanic transport. Recent studies suggest that Arctic river Hg inputs have been a potentially overlooked source of Hg to the AO. Observations on Hg in Eurasian rivers, which represent 80% of freshwater inputs to the AO, are quasi-inexistent, however, putting firm understanding of the Arctic Hg cycle on hold. Here, we present comprehensive seasonal observations on dissolved Hg (DHg) and particulate Hg (PHg) concentrations and fluxes for two large Eurasian rivers, the Yenisei and the Severnaya Dvina. We find large DHg and PHg fluxes during the spring flood, followed by a second pulse during the fall flood. We observe well-defined water vs. Hg runoff relationships for Eurasian and North American Hg fluxes to the AO and for Canadian Hg fluxes into the larger Hudson Bay area. Extrapolation to pan-Arctic rivers and watersheds gives a total Hg river flux to the AO of 44 ± 4 Mg per year (1σ), in agreement with the recent model-based estimates of 16 to 46 Mg per year and Hg/dissolved organic carbon (DOC) observation-based estimate of 50 Mg per year. The river Hg budget, together with recent observations on tundra Hg uptake and AO Hg dynamics, provide a consistent view of the Arctic Hg cycle in which continental ecosystems traffic anthropogenic Hg emissions to the AO via rivers, and the AO exports Hg to the atmosphere, to the Atlantic Ocean, and to AO marine sediments.

mercury | Arctic | rivers | ocean | modeling

Mercury (Hg), in its methylated form (MeHg), is an environmental toxicant that has been associated with long-term neurocognitive deficits in children and impaired cardiovascular health in adults (1, 2). Compared with other world regions, the Arctic is largely devoid of anthropogenic Hg emission point sources. Gaseous elemental Hg (GEM), the dominant form of Hg in emissions, has a long atmospheric lifetime (months) and can therefore be transported from emission-source regions to the Arctic (3). Thus, elevated Hg levels in Arctic biota have been linked to atmospheric transport of anthropogenic Hg emissions from the midlatitudes (3). The discovery of atmospheric Hg depletion events (AMDEs), depositing large amounts of atmospheric Hg to sea ice, reinforced a paradigm in which the atmosphere has a central role in shuttling Hg emissions to the Arctic marine environment (3, 4). The first Hg mass budget for the Arctic Ocean (AO) suggested a dominant role of atmospheric Hg deposition under steady-state conditions (5). Subsequent research has documented that between 60 and 80% of AMDE-deposited Hg is rapidly reduced and reemitted to the atmosphere (3). Recent studies using 3D coupled atmosphere–ocean models suggest that Arctic river inputs have been a potentially underestimated source of Hg to the AO (6, 7). The ratio of watershed to ocean basin surface is higher for the AO than for any other ocean basin (Fig. 1). Models, constrained by marine and atmospheric observations, suggest the AO to be a net source of Hg to the atmosphere (7–9) and have led to the suggestion that boreal soils and rivers are a key intermediate in trafficking midlatitude Hg emissions (via deposition to boreal soils) to the AO (10). Obrist et al. (11) documented how low Hg wet deposition to Arctic tundra is swamped by large annual atmospheric GEM uptake by tundra vegetation and soils, which potentially explains the large modeled river Hg flux. Model river Hg fluxes are severely underconstrained, however, with only a handful of low-water-stage Hg observations made on Eurasian rivers that represent 80% of Arctic river runoff (12, 13). Recent studies indicate that permafrost stores more Hg compared to other soils and oceans combined (11, 14). In the context of these findings and suggestions, understanding the Arctic Hg budget and AO Hg dynamics hinges on new observations of seasonal Eurasian river Hg fluxes.

Significance

Elevated levels of mercury in Arctic marine wildlife have been linked to midlatitude anthropogenic mercury emissions which are transported to the Arctic Ocean by air. Modeling studies, however, suggest that Arctic rivers contribute equal amounts of mercury to the Arctic Ocean. In this study, we provide comprehensive mercury data on large Eurasian rivers. We find that the spring flood mercury flux from Eurasian rivers is indeed large, which confirms a new Arctic mercury cycling paradigm: Mid-latitude anthropogenic emissions reach the terrestrial Arctic by air, whereby vegetation uptake transfers atmospheric mercury to tundra and boreal peat soils. Springtime snowmelt subsequently mobilizes peat soil mercury to the Arctic Ocean, where photochemistry drives net export of mercury back to the atmosphere.

Author contributions: J.E.S., R.T., L.-E.H.-B., and O.S.P. designed research; J.E.S., R.T., L.-E.H.-B., M.V.P., N.M., T.L.D., A.V.C., C.L., C.P.T., E.M.S., N.T., and O.S.P. performed research; J.E.S., R.T., C.P.T., E.M.S., and O.S.P. analyzed data; and J.E.S. wrote the paper.

The authors declare no conflict of interest.

This article is a PNAS Direct Submission.

Published under the PNAS license.

[1]To whom correspondence should be addressed. Email: jeroen.sonke@get.omp.eu.

This article contains supporting information online at www.pnas.org/lookup/suppl/doi:10.1073/pnas.1811957115/-/DCSupplemental.

Fig. 1. Map showing sampling locations (red dots) of the rivers Yenisei (at Igarka), S. Dvina (at Archangelesk), and G. Whale (at Kuujjuarapik). Gray areas reflect the majority of unmonitored watersheds for discharge. Adapted with permission from ref. 36, which is licensed under CC BY 4.0.

Coquery et al. (13) made unique total dissolved Hg (DHg) and particulate Hg (PHg) observations on the Lena, Ob, and Yenisei estuaries and river end members during the low-water stages of September 1991 and 1993. The authors observed low DHg values of 5.0, 2.8, and 1.5 pmol L^{-1} and low PHg values of 4.3, 34, and 1.1 pmol L^{-1} for the Lena, Ob, and Yenisei river end members, respectively. Annual DHg and PHg fluxes were estimated by taking into account water and sediment discharge and assuming that spring flood DHg is 3× higher than the September observations. A total Hg (THg = DHg + PHg) river flux of 6.0 Mg y^{-1} was computed for the Lena, Ob, and Yenisei and extrapolated to 15 Mg y^{-1} for total Eurasian river runoff into the AO (13). On the North American continent, river Hg concentrations have been more extensively observed for the Yukon, Mackenzie, Nelson, and Churchill rivers (15–18). Leitch et al. (16) estimated an annual THg) flux of 2.2 Mg y^{-1} for the Mackenzie River based on THg concentration measurements during the 2003–2005 spring floods. Concentrations of both DHg and PHg were up to 7× larger during peak flow than later in the year. Outridge et al. (5), in their AO Hg mass inventory, used these DHg and PHg observations to estimate an annual pan-Arctic THg river flux of 12.5 Mg y^{-1} (uncertainty range of 5.1 to 39.3 Mg y^{-1}).

Numerical models of global and Arctic Hg cycles have provided additional constraints on Arctic Hg fluxes and dynamics. Fisher et al. (7) used atmospheric GEM observations to constrain the coupled atmosphere–ocean GEOS-Chem simulation of Hg dynamics in the Arctic. The authors were able to reproduce the summertime rebound in GEM concentrations by invoking a missing source of Hg to the Arctic surface ocean from riverine inputs (7). Based on atmospheric observations and an initial parameterization for air–sea exchange of Hg^0 evasion, a terrestrial THg flux of ∼95 Mg y^{-1} (80 Mg y^{-1} from rivers and 15 Mg y^{-1} from coastal erosion) was needed to reproduce the observed summer GEM peak. Later work using an ocean model with more realistic physics and ecology for the Arctic lowered this estimate to a THg flux of 62 Mg y^{-1}, portioned into 46 Mg y^{-1} from rivers and 16 Mg y^{-1} from coastal erosion (8). A different modeling study suggested a lower river THg flux of 16 to 30 Mg y^{-1}, assuming that river Hg derives solely from atmospheric Hg(II) deposition (19).

Large annual pan-Arctic river THg fluxes have also been estimated by extrapolating Hg/dissolved organic carbon (DOC) observations and DOC river budgets. Kirk and St Louis (15) examined DHg, PHg, dissolved MeHg (DMeHg), and DOC inputs from the Nelson and Churchill rivers into Hudson Bay for the period 2003–2007. Schuster et al. (17) measured DHg, PHg, and DOC export from the Yukon River to the Bering Sea from 2001 to 2005 and observed a mean THg flux of 4.4 Mg y^{-1}, mainly driven by elevated PHg. The authors noticed strong correlations between DHg and DOC (r^2 = 0.81) and between PHg and POC (r^2 = 0.50). Kirk et al. (20) estimated riverine export of THg to Arctic and sub-Arctic waters of 108 Mg y^{-1}, based on the correlations of DOC with DHg/DOC and DHg/THg ratios for the Yukon River. Dastoor and Durnford (6) revised the North American DHg/DOC relationship for a potential Hg contribution from historical gold mining in Alaska to the Yukon River by including DHg/DOC data for the Mackenzie River; they proposed an annual THg flux to the AO of 50 Mg y^{-1}, with large uncertainty in the DOC budget. Amos et al. (12) constructed a global budget for riverine Hg inputs to the oceans and included new data on THg concentrations in Eurasian rivers. River end-member samples were collected every other month during 2012–2013 in the Ob (n = 7), Lena (n = 7), Yenisei (n = 6), and Kolyma (n = 7) estuaries, and the respective mean THg concentrations of 24, 39, 18, and 14 pmol L^{-1} were 3× times higher than the early 1990s observations (13). Based on the available concentration data and number of samples collected, Amos et al (12) reported a THg flux of 8 Mg y^{-1} to the AO. In summary, observation and modeling-based estimates of Arctic river THg fluxes range from 8 to 108 Mg y^{-1} and are limited by THg and/or DOC observations on Eurasian rivers.

In this study, we present seasonal observations on DHg, PHg, DOC, and select DMeHg concentrations and fluxes for two large Eurasian rivers: the Yenisei and the Severnaya Dvina (S. Dvina). We provide additional observations on a smaller river, the Great Whale (G. Whale) River in Canada, to better constrain THg runoff into the Hudson Bay. We interpolate and extrapolate our comprehensive observations to the larger Arctic watershed and use a 3D model (8) to assess net sea–air exchange of Hg over the AO. We then use our revised Arctic river Hg flux together with observations on tundra Hg dynamics and AO Hg observations to revisit the Arctic Hg budget and cycling.

Materials and Methods

Sampling and Analysis. The AO watersheds and the Yenisei, S. Dvina, and G. Whale rivers are represented in Fig. 1. Hg samples were filtered in the field using preburnt quartz filters and a Teflon filter holder into acid-cleaned 500 mL fluorinated ethylene propylene Teflon bottles, acidified to 0.36 M HCl, and stored cold and in the dark until transport to France for analysis. DHg is defined here as the sum of inorganic and MeHg in the filtrate. PHg is defined as the inorganic and MeHg fraction retained on the quartz filter. DHg was measured by atomic fluorescence spectrometry following the US Environmental Protection Agency Method 1631 (21). We measured DMeHg as the sum of monomethyl (MM)Hg and dimethylmercury in the filtrate. DMeHg was analyzed via isotope dilution using GC-inductively coupled plasma-MS (21). Whole quartz filters were analyzed for PHg by combustion cold vapor atomic absorption spectrometry (Milestone DMA-80). DOC was measured on a Shimadzu TOC-VCSN Analyzer. Full details on all methods, including quality assurance/control and blanks, can be found in *SI Appendix, Supplementary Text*.

Flux Calculations. Our 2012–2016 observations for DHg, PHg, and THg concentrations were multiplied by daily water discharge (from Roshydromet) to obtain daily Hg fluxes, which were then interpolated and integrated to estimate annual Hg fluxes. Data interpolation was performed using discharge vs. DHg, PHg, or THg concentration or yield trends, following published

guidelines (17). DMeHg was measured only during the 2012 spring flood for the S. Dvina (April to August) and the G. Whale (May) rivers. Correlations between DHg and DMeHg are used to estimate S. Dvina DMeHg concentration and fluxes from January to March and from September to December.

Air–Sea Exchange Modeling. We simulated Hg^0 evasion from the AO configuration of the Massachusetts Institute of Technology general circulation model (MITgcm). The MITgcm includes carbon cycling and plankton dynamics and has a horizontal resolution of 36 km and 50 vertical ocean layers, with a coupled sea-ice model, and boundary conditions from a 1° × 1° global simulation (15). The oceanic Hg simulation was forced using atmospheric Hg^0 concentrations and Hg deposition from the GEOS-Chem atmospheric chemical transport model (8). We use the model to assess the impact of Arctic riverine Hg discharges on AO Hg^0 evasion to the atmosphere.

Results and Discussion

Observations on discharge ($m^3\ s^{-1}$) and concentrations of DOC (mg L^{-1}) and DHg, PHg, THg, and DMeHg (pmol L^{-1}) are summarized in Dataset S1.

2012–2013 S. Dvina Hg and DOC. Seasonal discharge for the S. Dvina River peaks during the spring and fall floods, and total annual discharge varied substantially between 2012 (128 $km^3\ y^{-1}$) and 2013 (85 $km^3\ y^{-1}$) (Fig. 2). DOC levels in the S. Dvina during base flow (5.6 mg L^{-1}) and spring flood (18 mg L^{-1}) were typical of Russian boreal rivers (22). Base flow DHg, PHg, and THg levels were 3.8, 19.9, and 23.7 pmol L^{-1}; spring flood DHg, PHg, and THg levels were up to 52, 55, and 107 pmol L^{-1}; and fall flood DHg, PHg, and THg levels were up to 68, 39 and 107 pmol L^{-1}, respectively (Fig. 2). DHg, PHg, and THg are all correlated with discharge (r^2 values of 0.31, 0.50, and 0.54, respectively) and with DOC (r^2 values of 0.69, 0.23, and 0.48, respectively), similar to previous observations on North American rivers (17) (*SI Appendix*, Fig. S1 *A* and *B*). DMeHg was measured in 2012 and ranged from 0.25 to 0.87 pmol L^{-1}, representing 1 to 4% of DHg (Fig. 2). DMeHg was anticorrelated with DHg ($r^2 = 0.40$) and discharge ($r^2 = 0.75$), but not with DOC ($r^2 = 0.11$). Low DHg and elevated

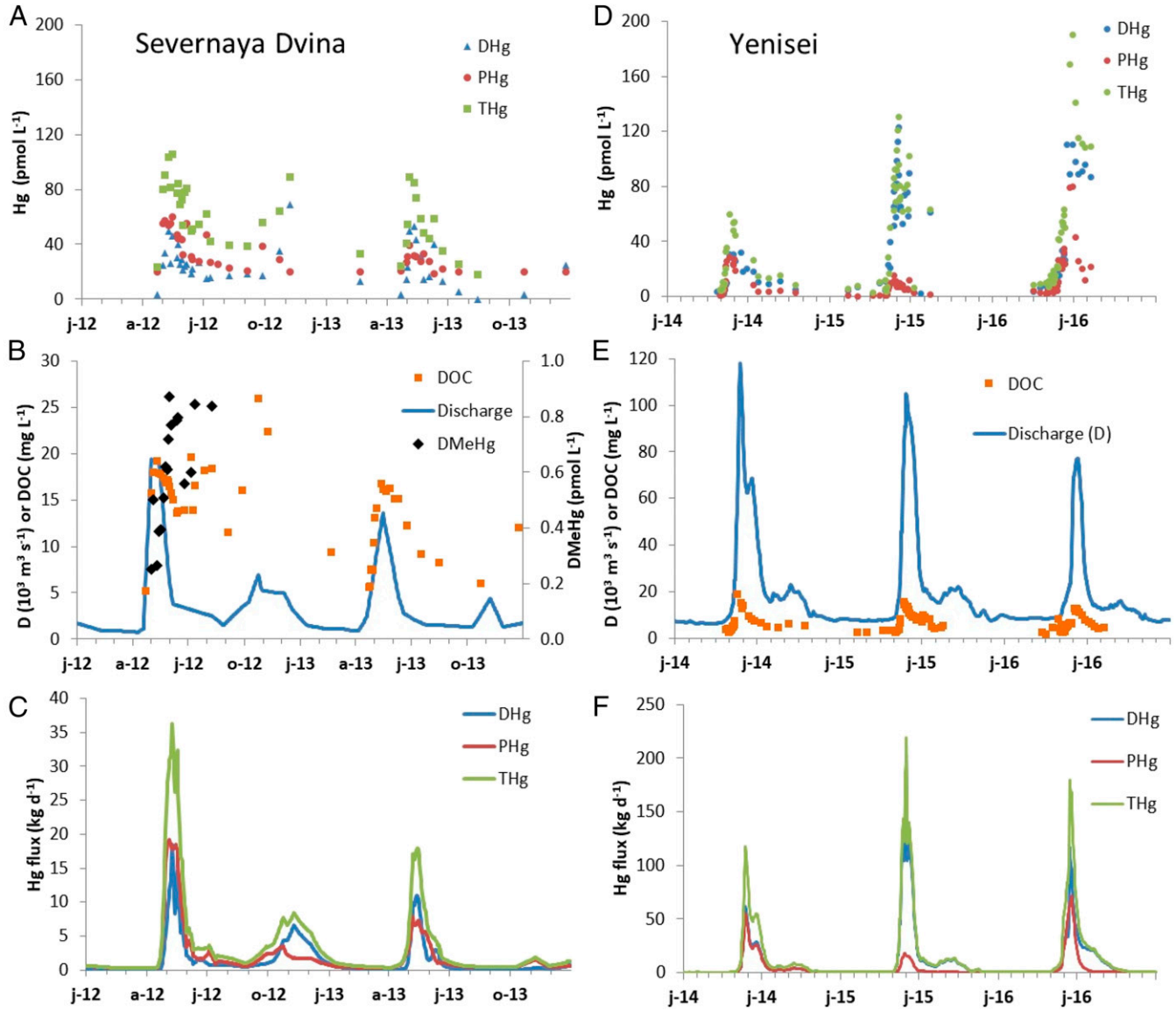

Fig. 2. (*A–F*) Observations in 2012 and 2013 on the S. Dvina River (*A–C*) and in 2014, 2015, and 2016 on the Yensei River (*D–F*) for DHg, PHg, and THg (*A* and *D*), DMeHg (*B*), as well as discharge (D) and DOC (*B* and *E*). Interpolation of Hg concentrations and discharge gives Hg fluxes (*C* and *F*). The S. Dvina dates indicate month and year, with j, a, j, and o corresponding to January, April, July, and October, respectively. Yenisei dates indicate January (j-14), July (j-14), January (j-15), etc.

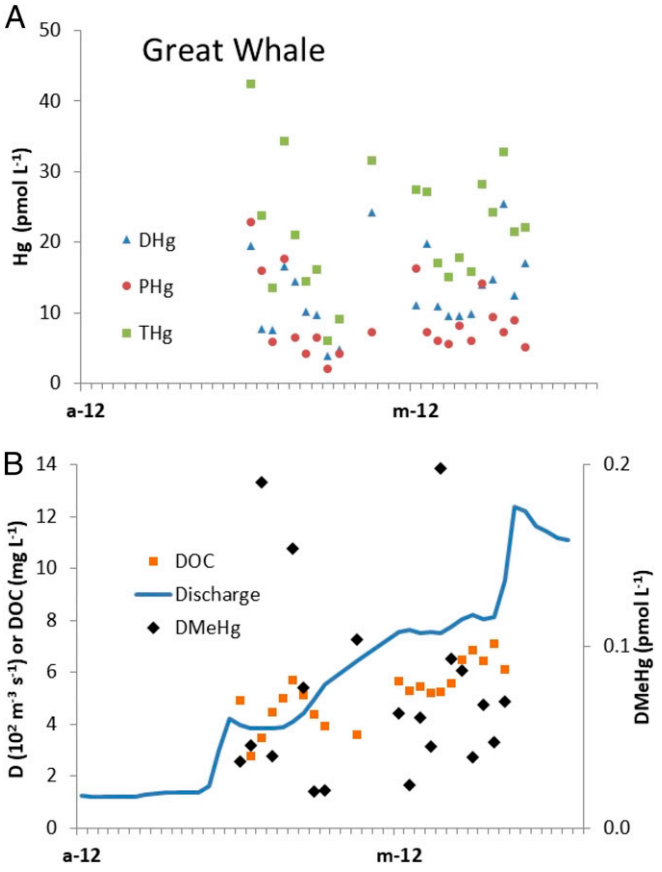

Fig. 3. (*A* and *B*) Observations in 2012 on the G. Whale River during spring flood [April (a) and May (m) 2012] for DHg, PHg, and THg (*A*) and for DMeHg, discharge (D), and DOC (*B*).

PHg during S. Dvina base flow are similar to Coquery et al.'s (13) DHg (2.8 pmol L^{-1}) and PHg (34 pmol L^{-1}) observations for the Ob river, reflecting similar watershed characteristics.

2014–2016 Yenisei Hg and DOC. Annual water discharge for the Yenisei River, at Igarka, in 2014 and 2015 was similar (634 and 618 km^3 y^{-1}, respectively), but lower in 2016 (482 km^3 y^{-1}) (Fig. 2). DOC levels in the Yenisei during base flow (3.9 mg L^{-1}) and spring flood (19 mg L^{-1}) were similar to those of the S. Dvina River. Base flow DHg, PHg, and THg were 3.6, 3.2, and 6.8 pmol L^{-1}; spring flood DHg, PHg, and THg levels were up to 123, 80, and 191 pmol L^{-1}; and fall flood DHg, PHg, and THg levels were up to 62, 4, and 64 pmol L^{-1}, respectively (Fig. 2). DHg, PHg, and THg are correlated with discharge (r^2 values of 0.80, 0.74, and 0.86, respectively) and with DOC (r^2 values of 0.87, 0.75, and 0.92, respectively) (*SI Appendix*, Fig. S1 *A* and *B*). DMeHg was not measured in the Yenisei samples. Our base flow THg observations of 6.8 ± 2.5 pmol L^{-1} are slightly higher than the September 1993 observations of 2.6 pmol L^{-1} by Coquery et al. (13), which may reflect year-to-year variation. Our spring flood maximum THg level (191 pmol L^{-1}) is well above the extrapolated 3× 2.6 pmol L^{-1} spring flood level. Annual DHg, PHg, and THg levels were unexpectedly variable by factors of 2 to 3 and possibly related to annual variability in snowmelt and water runoff dynamics.

2012 G. Whale Hg and DOC. The daily observations during the 2012 G. Whale River spring flood provide a high-resolution view of Hg and DOC discharge from a watershed that is 8× or 56× smaller than that of the S. Dvina or Yenisei rivers, respectively. Fig. 3*A* illustrates three pulsed increases in discharge as different regions within the G. Whale watershed progressively undergo snow melt. Within the first two snow melt and discharge pulses, DHg, PHg, DMeHg, and THg (but not DOC) are nonlinearly anticorrelated with discharge, suggesting a flushing effect of the Hg carrying phases. Consequently, THg is not correlated with discharge (r^2 = 0.03) over the entire month of observations. Similarly weak THg vs. discharge correlations were made for the Nelson and Churchill rivers (r^2 values of 0.05 and 0.34, respectively) that also run off into Hudson Bay (23). Further identification of the underlying hydrogeochemical dynamics for the G. Whale is beyond the scope of this study. Due the progressive increase in discharge during the spring flood, THg yield does correlate well with runoff and is similar among the Nelson, Churchill, and G. Whale rivers (see below).

Arctic River Hg Fluxes by Hg/DOC Extrapolation. Three different extrapolation methods can be used to estimate circum-Arctic river Hg fluxes. All critically depend on accurate estimates of freshwater discharge into the seas that make up the AO. The simplest method uses water discharge-weighted average Hg concentrations for select Arctic rivers and extrapolates these to the entire Arctic watershed using total discharge budgets (5, 12). The second method uses THg/DOC observations on select rivers multiplied by pan-Arctic DOC fluxes (which combine DOC observations and discharge) (6, 20). The third method, well-illustrated for a recent estimate of the Arctic river DOC flux (22), combines seasonal observations of Hg on multiple rivers to derive relationships between drainage area (km^2)-normalized discharge (water yield, or runoff in cm y^{-1}) and Hg yield (i.e., Hg runoff in $\mu g \cdot m^{-2} \cdot y^{-1}$). In this study, we use the second and third methods to derive estimates for annual and daily riverine DHg, PHg, THg, and DMeHg inputs into the AO and Hudson Bay. An important aspect of these methods is the correction to be made for the 33.1% of Arctic watersheds that are not monitored for water discharge, DOC, and Hg (24). We provide separate estimates of THg flux to the AO from Eurasian and North American rivers and to the larger Hudson Bay area (i.e., Hudson Bay, Hudson Strait, James Bay, and Ungava Bay). We do not include Hg runoff to the Bering Sea, as Hg transport from the Pacific Ocean to the AO is taken into account separately in previous AO Hg budgets (5, 9).

DOC fluxes from North American and Russian rivers are historically better documented than Hg fluxes, in particular by the international Pan-Arctic River Transport of Nutrients, Organic Matter and Suspended Sediments (PARTNERS) program (22). Previous studies have used observations on THg/DOC ratios from the North American Yukon and Mackenzie rivers, together with pan-Arctic DOC fluxes, to estimate river THg fluxes to the AO of 108 Mg y^{-1} (20) and 50 Mg y^{-1} (6). Uncertainties in these estimates arise mainly from extrapolating THg/DOC ratios for North American rivers to Eurasian rivers and from uncertainty in DOC fluxes. In addition, the Yukon River has been suggested to have unnaturally high PHg/DOC and THg/DOC ratios due to the impact of legacy gold mining (6). In the absence of representative THg/DOC observations on Eurasian rivers, a key assumption in these studies has been that North American THg/DOC ratios apply to Eurasian rivers. *SI Appendix*, Table S1 summarizes THg/DOC ratios for the Mackenzie, Nelson, Churchill, Yenisei, S. Dvina, and G. Whale rivers. We observe that THg/DOC ratios for Yenisei and S. Dvina are lower (mean of 1.15 Mg Tg^{-1}) than for the Mackenzie (2.59 Mg Tg^{-1}). THg/DOC ratios for the Hudson Bay, based on Nelson, Churchill, and G. Whale rivers, are lowest of all at 0.27 Mg Tg^{-1}. Consequently, the extrapolation of North American THg/DOC ratios to Eurasian boreal rivers has led to an overestimation of THg flux to the AO (6, 20). To estimate THg fluxes to the AO, we used an Arctic DOC flux of 35.4 Tg y^{-1} from Manizza et al. (25) that is based on PARTNERS data (22), corrected for unmonitored high-latitude watersheds that are thought to have high DOC runoff (25). We assume that river runoff into the East Siberian and Chukchi seas has intermediate THg/DOC (and DHg/THg) values (see *SI*

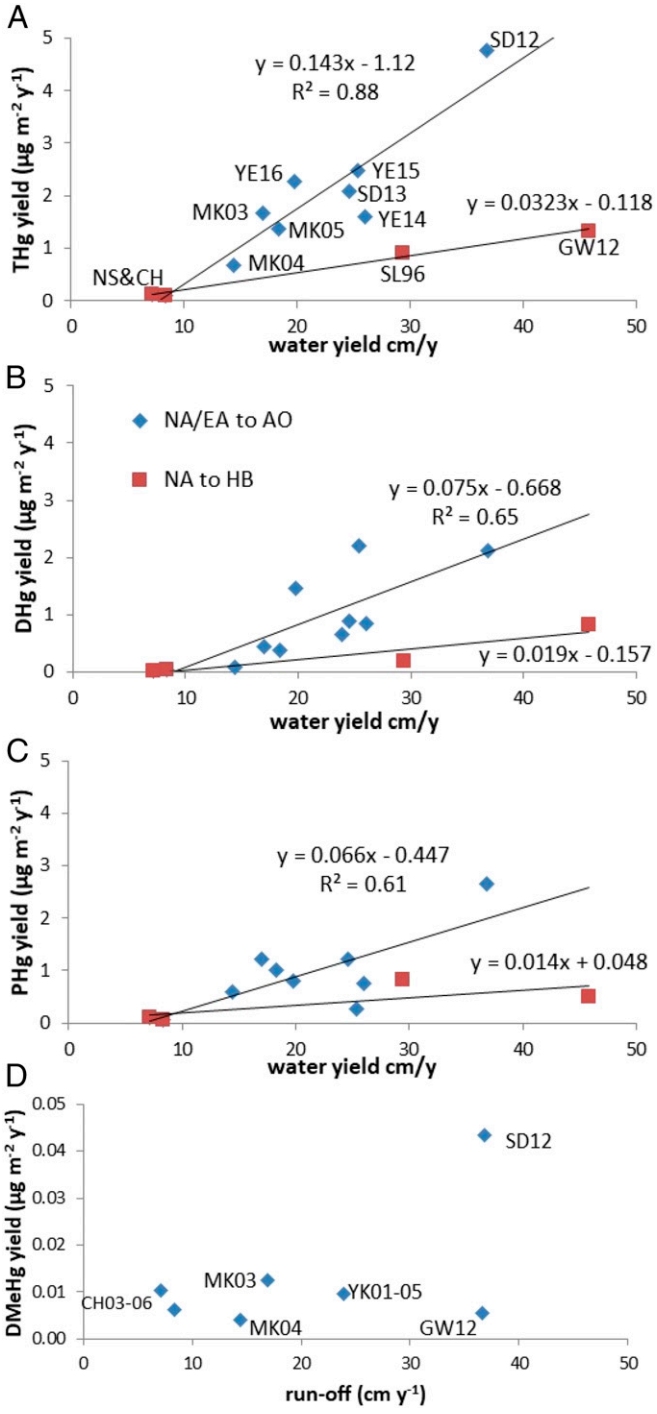

Fig. 4. (*A–D*) Relationships between annual water and Hg runoff. Annual Hg yield ($\mu g \cdot m^{-2} \cdot y^{-1}$) as a function of river runoff (cm y^{-1}) for North American (NA) and Eurasian (EA) watersheds to the AO and for the NA watershed to the larger Hudson Bay (HB). Year of observation is coded with rivers, which are abbreviated as follows: CH, Churchill; GW, G. Whale; MK, Mackenzie; NE, Nelson; SL, Saint Lawrence; SD, S. Dvina; and YE, Yenisei. The SL does not run off into the HB but is included in the linear regressions. The regressions were used to estimate annual THg (*A*), DHg (*B*), PHg (*C*), and DMeHg (*D*) fluxes for 112 pan-Arctic rivers for which discharge and watershed area are documented (Dataset S2).

Appendix, Table S2) that are between our Yenisei and S. Dvina river and North American river observations, based on continental lithology, geomorphology, and sediment discharge. We use our revised THg/DOC (and DHg/THg) ratios in *SI Appendix*, Table S1 to estimate a DOC-based pan-Arctic THg flux of 43 Mg y^{-1} (*SI Appendix*, Table S2). This flux is similar to the previous THg/DOC-based estimate of 50 Mg y^{-1} by Dastoor and Durnford (6), because our lower Eurasian THg/DOC ratios are offset by the larger DOC flux of 35.4 Tg y^{-1} that we use (compared with the 21.2 Tg y^{-1} uncorrected DOC flux in ref. 6).

Arctic River Hg Fluxes by Extrapolation of Watershed Hg Yields. Since DHg, PHg, and THg correlate with river discharge, we can use an alternative and more direct method to scale up the Yenisei, S. Dvina, G. Whale, and published Hg observations to all Arctic watersheds. Fig. 4 *A–C* shows the relationships between annual THg, DHg, and PHg flux and discharge, both normalized to watershed area, to give annual THg, DHg, and PHg yield ($\mu g \cdot m^{-2} \cdot y^{-1}$) and water yield (runoff, cm y^{-1}). Published Hg fluxes for the Mackenzie River in 2003–2005 (16), the Nelson and Churchill rivers in 2003–2007 (15), and the Saint Lawrence River (26) are included. Yukon River observations (17) are not included because of the anthropogenic impact on its river basin (see ref. 6 and below). Annual Hg yields correlate well with water yields for all North American and Eurasian rivers that drain into the AO (NA/EA→AO) (Fig. 4 *A–C*). An exception to the trends are the low Hg yields of the G. Whale and Saint Lawrence watersheds on the eastern Hudson Bay (Fig. 4 *A–C*). This observation is not trivial because North Quebec, which drains into the eastern Hudson Bay and Atlantic Ocean, has among the highest wet precipitation and runoff across the entire (sub)Arctic (27). Extrapolating the linear NA/EA→AO relationship to the eastern Hudson Bay, where 20 rivers have water yields >40 cm y^{-1} (37% of Canadian runoff), would result in a large, overestimated THg flux to the Hudson Bay and Strait. We therefore separated Hg- and water-yield relationships into (*i*) a North American/Eurasian component based primarily on the S. Dvina, Yenisei, and Mackenzie observations, but also including the Nelson and Churchill rivers, which drain watersheds on the drier, western Hudson Bay, and (*ii*) a Hudson Bay (and Strait) component that is based on a linear regression of the same Nelson and Churchill river data, as well as the G. Whale and Saint Lawrence river data. Although the Saint Lawrence River does not run off into the Hudson Bay (but into the Atlantic Ocean), it has similar watershed climate, land use, and low Hg yield as compared to the G. Whale, justifying our separation of Hudson Bay Hg runoff from the rest of North America. Based on Fig. 4 *A–C*, Hg yields can be formulated as follows:

$$(Y_{THg})_{NA/EA\rightarrow AO} = 0.143 \times (R) - 1.121 \quad [1]$$

$$(Y_{DHg})_{NA/EA\rightarrow AO} = 0.0745 \times (R) - 0.668 \quad [2]$$

$$(Y_{PHg})_{NA/EA\rightarrow AO} = 0.0663 \times (R) - 0.447 \quad [3]$$

$$(Y_{THg})_{HB} = 0.032 \times (R) - 0.118 \quad [4]$$

$$(Y_{DHg})_{HB} = 0.014 \times (R) \quad [5]$$

$$(Y_{PHg})_{HB} = 0.014 \times (R) + 0.048, \quad [6]$$

where Y is the annual yield of DHg, PHg, and THg ($\mu g \cdot m^{-2} \cdot y^{-1}$); R is the annual runoff for a given watershed (cm y^{-1}); and HB is the Hudson Bay. Hg yield and runoff are defined as

$$Y_{THg} = (10^3 \times F_{THg}/A) \quad [7]$$

$$R = D/A \times 10^5 \quad [8]$$

Table 1. Summary of modeled and observed THg, DHg, and PHg fluxes for the 10 largest Arctic rivers generating 80% of the THg flux to the AO

River	Discharge,* $km^3\ y^{-1}$	Area,* $10^3\ km^2$	THg mod, $Mg\ y^{-1}$	DHg mod, $Mg\ y^{-1}$	PHg mod, $Mg\ y^{-1}$	THg obs,† $Mg\ y^{-1}$	DHg obs,† $Mg\ y^{-1}$	PHg obs,† $Mg\ y^{-1}$	THg obs/mod‡	DHg obs/mod‡	PHg obs/mod‡
Yenisei	606	2533	5.8	2.8	2.8	5.2	3.7	1.5	0.9	1.3	0.5
Lena	534	2453	4.8	2.3	2.4						
Ob	411	2522	2.5	1.1	1.4						
Mackenzie	285	1671	2.2	1.0	1.1	2.4	0.7	1.8	1.1	0.6	1.5
Pechora	143	324	1.7	0.9	0.8						
Khatanga	139	437	1.6	0.8	0.8						
S. Dvina	110	368	1.2	0.6	0.6	1.2	0.5	0.7	1.0	0.9	1.2
Kolyma	116	627	0.93	0.44	0.48						
Taz	54.7	167	0.60	0.30	0.29						
Indigirka	54.5	329	0.37	0.17	0.20						
Mean									1.0	0.9	1.1
1σ§									0.1	0.3	0.5
Yukon¶	203	850	2.0	1.0	1.0	4.4	0.6	3.8	2.2	0.6	4.0

mod, modeled; obs, observed.
*Discharge and watershed area at the river mouth are from Dai and Trenberth (24).
†Observed fluxes are mean values for the years of observation.
‡Mean observed/modeled ratios suggest the regression model (Eqs. **1**–**6**) to be unbiased with respect to observations.
§1σ SDs are suggested to represent multiannual model uncertainty.
¶The Yukon River, running off into the Bering Sea, is shown separately to illustrate its anthropogenic observed/modeled PHg ratio of 4.

where F is the annual flux of THg, DHg, and PHg ($kg\ y^{-1}$); A is the watershed area (km^2); and D is the annual discharge ($km^3\ y^{-1}$). Using Eqs. **1**–**8** together with published discharge and watershed area data for 116 Arctic rivers (24, 28), we estimate annual pan-Arctic DHg, PHg, and THg fluxes of 22, 22, and 44 $Mg\ y^{-1}$, respectively (Dataset S2). The 10 largest Hg contributing rivers to the AO are summarized in Table 1. In calculating these fluxes, we correct discharge for the "river mouth to station" flow-rate ratios (24), and use corresponding watershed surface area at the river mouth. Dai and Trenberth (24) estimated that, on average, 33.1% of Arctic watersheds are unmonitored for discharge, which we also correct for ref. 24. DOC fluxes from the relatively smaller unmonitored high-latitude watersheds are thought to be enhanced (25). Hg fluxes from unmonitored watersheds are therefore also likely enhanced. This is confirmed in *SI Appendix*, Fig. S2, which shows more elevated THg yields for smaller watersheds throughout Eurasia. We therefore use mean THg yield for watersheds <10,000 km^2 to estimate THg fluxes from unmonitored watersheds (Table 2). Our revised, and recommended, THg flux of 44 $Mg\ y^{-1}$ is similar to our Hg/DOC-based THg flux of 43 $Mg\ y^{-1}$. Similarly, DHg and PHg make up 50% each of the THg flux in both estimates.

We estimate the uncertainty of the yield-based pan-Arctic Hg river flux of 44 $Mg\ y^{-1}$ by comparing the annual Hg fluxes from the regression model to the observed annual Hg fluxes for the three largest rivers with observations—the Yenisei, Mackenzie, and S. Dvina (Table 1). On average, multiannual model DHg, PHg, and THg fluxes are unbiased against observations within 10%. The multiannual 1σ uncertainties associated with model DHg, PHg, THg flux estimates are 35%, 48%, and 10%, respectively. Our revised river THg flux of $44 \pm 4\ Mg\ y^{-1}$ (1σ) and the recently revised erosion Hg flux of 30 $Mg\ y^{-1}$ (9) agree (within uncertainty) with the model-based estimates of Zhang et al. (8). The revised annual budget will likely allow further refinement of other uncertainties in Arctic Hg models, such as evasion to the atmosphere and Hg export flux to the shelf and deep AO.

Daily River Hg Flux Regression Equations. Our observations will also allow a much finer temporal (i.e., daily) assessment of Hg fluxes to the AO, which are addressed below. Fig. 5 explores the relationships between daily DHg, PHg and THg flux and daily discharge, again normalized to watershed area, to give daily DHg, PHg, and THg yield ($ng{\cdot}m^{-2}{\cdot}d^{-1}$) and water yield (runoff, $cm\ d^{-1}$). As before, we separated Hg inputs to the AO from inputs to the larger Hudson Bay. The observed correlations are good (r^2 values of 0.81 to 0.91) and again provide the possibility to couple Hg fluxes directly to daily gridded water discharge and watershed area in Arctic Hg models:

Table 2. Summary of annual pan-Arctic river Hg fluxes to the AO

Region	Discharge, $km^3\ y^{-1}$	Watershed area, $10^3\ km^2$	THg yield, $\mu g{\cdot}m^{-2}{\cdot}y^{-1}$	DHg yield, $\mu g{\cdot}m^{-2}{\cdot}y^{-1}$	PHg yield, $\mu g{\cdot}m^{-2}{\cdot}y^{-1}$	DMeHg yield, $\mu g{\cdot}m^{-2}{\cdot}y^{-1}$	THg flux, $Mg\ y^{-1}$	DHg flux, $Mg\ y^{-1}$	PHg flux, $Mg\ y^{-1}$	DMeHg flux, $Mg\ y^{-1}$
Water discharge monitored										
Eurasia	2452	10962					22.8	11.1	11.3	0.47
North America	364	2056					2.9	1.4	1.5	0.088
Hudson Bay	717	3014					2.0	1.0	1.1	0.024
Unmonitored										
Eurasia	812	3629	3.88	1.96	1.86	0.043	14	7.1	6.8	0.16
North America	120	681	1.64	0.90	0.83	0.043	1.1	0.61	0.56	0.029
Hudson Bay	237	998	1.21	0.57	0.62	0.008	1.2	0.57	0.62	0.008
Total (Hg yield-based)							**44.1**	**21.7**	**21.9**	**0.78**
Total (Hg/DOC-based)							43.0	21.5	21.5	

Discharge data for 112 monitored watersheds (Dataset S2) and the linear regression model (Eqs. **1**–**8**) provide Hg yield observation-based flux estimates. Recommended values are shown in bold.

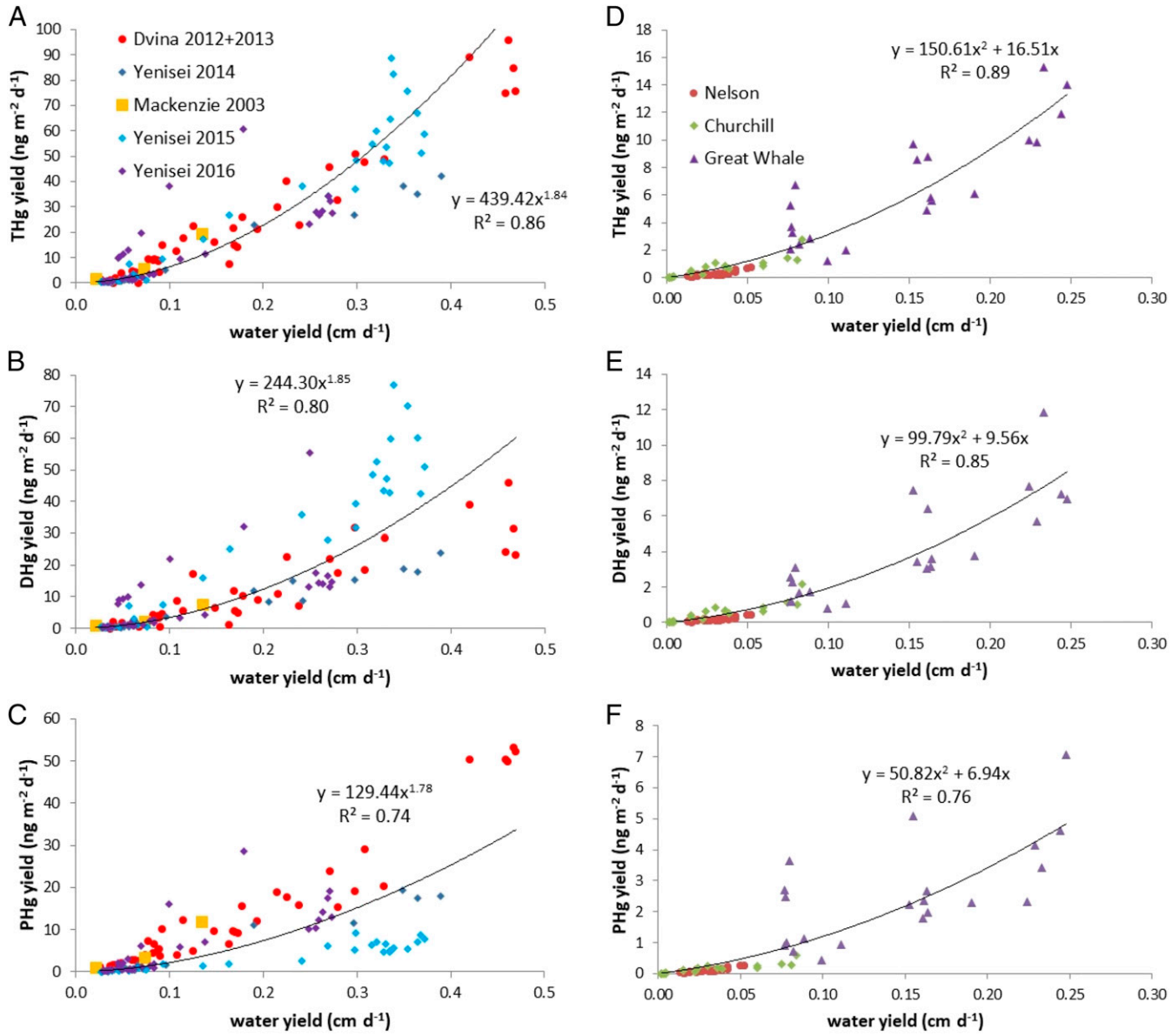

Fig. 5. (*A–F*) Relationships between daily water and Hg runoff. Daily Hg yield (ng·m^{-2}·d^{-1}) as a function of river runoff (cm d^{-1}) for North American and Eurasian watersheds (*A–C*) and Hudson Bay (*D–F*). The polynomial regressions can be used to estimate daily river fluxes for THg (*A* and *D*), DHg (*B* and *E*), and PHg (*C* and *F*) across the Arctic when daily discharge and watershed area are known. Data for the Mackenzie, Nelson, and Churchill rivers are from refs. 7 and 8.

$$\left(Y_{THg}\right)_{NA/EA\rightarrow AO} = 439.4 \times (R)^{1.838} \quad [9]$$

$$\left(Y_{DHg}\right)_{NA/EA\rightarrow AO} = 244.3 \times (R)^{1.853} \quad [10]$$

$$\left(Y_{PHg}\right)_{NA/EA\rightarrow AO} = 129.4 \times (R)^{1.782} \quad [11]$$

$$\left(Y_{THg}\right)_{HB} = 0.036 \times (R) – 0.164 \quad [12]$$

$$\left(Y_{DHg}\right)_{HB} = 0.021 \times (R) – 0.131 \quad [13]$$

$$\left(Y_{PHg}\right)_{HB} = 0.015 \times (R) – 0.033, \quad [14]$$

where Y is the daily yield of THg, DHg, and PHg (ng·m^{-2}·d^{-1}); and R is the daily runoff for a given watershed (cm d^{-1}).

Arctic River MeHg Fluxes. Although DMeHg fluxes were not the primary objective of our study, we performed measurements on filtered samples from the G. Whale and S. Dvina rivers during the 2012 spring floods. Examination of the DMeHg observations together with those published in the literature allows some level of extrapolation on annual timescales, albeit with larger uncertainties than for THg. The G. Whale DMeHg level is low [0.074 ± 0.038 pmol L^{-1} (1σ)]; is not correlated to DHg, DOC, or discharge; and is lower than previous observations in the Nelson and Churchill rivers [0.37 and 0.73 pmol L^{-1}, respectively (15)] that drain watersheds on the western Hudson Bay. The S. Dvina DMeHg levels are higher [0.59 ± 0.16 pmol L^{-1} (1σ)], similar to those observed in the Nelson, Churchill, Mackenzie, and Yukon rivers [0.38, 0.73, 0.38, and 0.20 pmol L^{-1}, respectively (12–14)]. S. Dvina DMeHg anticorrelates sufficiently well with DHg (r^2 = 0.40, *SI Appendix*, Fig. S1*C*) so that we can use this relationship to roughly estimate pre- and postflood DMeHg levels to estimate an annual DMeHg flux of 15.1 kg y^{-1}.

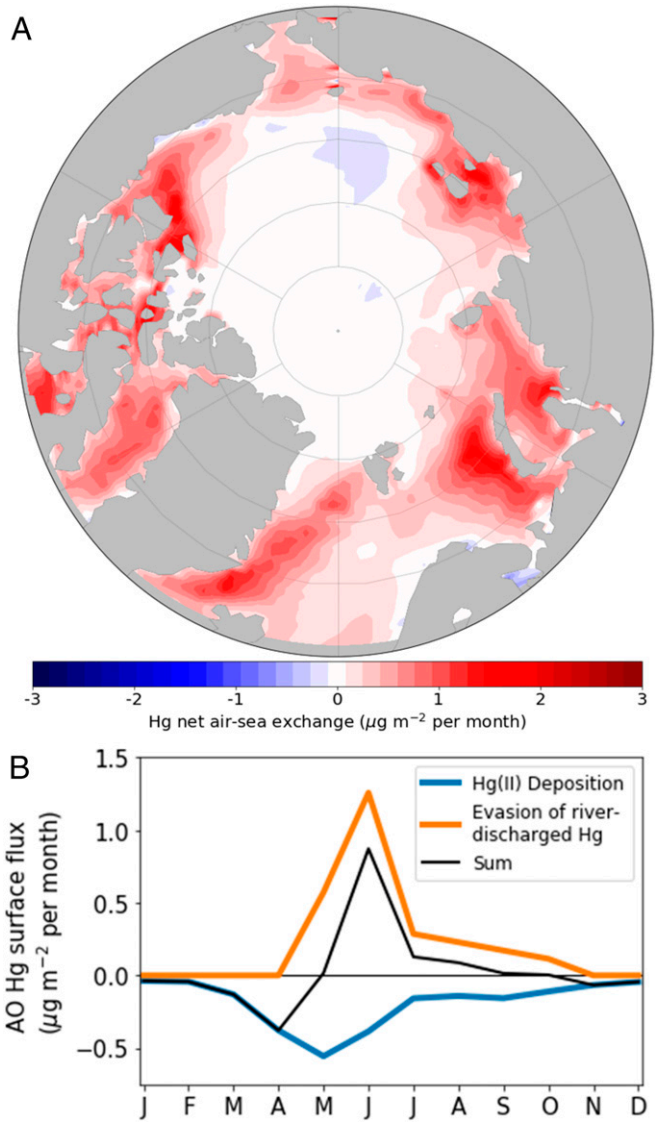

Fig. 6. (*A* and *B*) Modeled net air–sea exchange of Hg ($\mu g \cdot m^{-2} \cdot mo^{-1}$) across the AO basin for the months June-July (*A*) and seasonally integrated (*B*) from the coupled GEOS-Chem/MITgcm Hg chemistry and transport model. Letters on the *x* axis correspond to months of the year.

Similar to DHg, PHg, and THg, we can explore annual DMeHg yield vs. runoff relationships (Fig. 4*D*). We observe no trend in annual DMeHg yield vs. runoff, apart from the Eurasian S. Dvina having a higher yield of 0.043 $\mu g \cdot m^{-2} \cdot y^{-1}$ than North American rivers (0.008 ± 0.003 $\mu g \cdot m^{-2} \cdot y^{-1}$), presumably due to much higher DOC in the former. In the absence of additional Eurasian river data, we constrain North American/Eurasian and Hudson Bay yields for DMeHg to the AO to be independent of runoff:

$$(Y_{DMeHg})_{NA/EA \rightarrow AO} = 0.0043 \text{ μg m}^{-2}\text{y}^{-1}$$

$$(Y_{DMeHg})_{HB} = 0.008 \text{ μg m}^{-2} \text{ y}^{-1},$$

where Y is the annual yield of DMeHg ($\mu g \cdot m^{-2} \cdot y^{-1}$). Extrapolation to all 116 Arctic rivers and correcting for 33.1% unmonitored Arctic watersheds gives an annual DMeHg flux of 0.78 Mg y^{-1}. This corresponds to an average DMeHg fraction of 1.7%. Although we did not measure particulate MMHg (PMMHg) levels, we estimate these to be 0.019 Mg y^{-1} based on our DMeHg flux of 0.78 Mg y^{-1} and the MMHg logK_d of 2.7 L kg^{-1} and the 2.27 10^8 Mg y^{-1} Arctic river sediment flux (9). Our total MeHg (TMeHg = DMeHg + PMMHg) flux of 0.80 Mg y^{-1} is lower than previous estimates of 2.5 Mg y^{-1} that were based on an average TMeHg/THg fraction of 5% (1 to 10% range) and THg flux of 46 Mg y^{-1} (9).

Implications for Arctic Hg Cycling. Fisher et al. (7) hypothesized that the summer rebound in Arctic atmospheric GEM could be explained by a large riverine flux of Hg to the AO and associated peak in marine Hg evasion to the atmosphere. Subsequent work by Zhang et al. (8), which coupled the atmospheric simulation from Fisher et al. (7) with a 3D ocean simulation for the Arctic, suggested that a lower input from Arctic rivers of 46 Mg y^{-1} would be sufficient to explain the summertime peak in atmospheric GEM concentrations. Riverine Hg flux estimates into the AO were relatively unconstrained before the observations presented in this work due to lack of data from the Eurasian Arctic rivers. Our observationally based estimate of AO river inputs (44 ± 4 Mg y^{-1}) agrees with prior modeling estimates, presenting a consistent picture of Hg dynamics in the Arctic.

The magnitude of the riverine Hg flux shown in this study leads to enhanced evasion in the AO in summer (Fig. 6*A*, June to July), which is sufficient to explain the summertime rebound in coastal AO atmospheric GEM concentrations. Net air–sea exchange of Hg is strongest over the continental shelf areas due to heat transfer from continental regions and turbulence from sea-ice rafting (8). Evasion is inhibited in the central AO due to the presence of sea ice. The seasonal dynamics of air–sea exchange of Hg are shown in Fig. 6*B* and illustrate how marine evasion of river-discharged Hg exceeds Hg deposition from May to August, after the spring flood.

Based on the ensemble of these observations and model studies, Fig. 7 summarizes the essential features of the modern Arctic Hg cycle. Midlatitude atmospheric Hg emissions are transported to the Arctic where terrestrial vegetation and soil Hg^0 uptake drives a large net Hg deposition of 210 Mg y^{-1} to

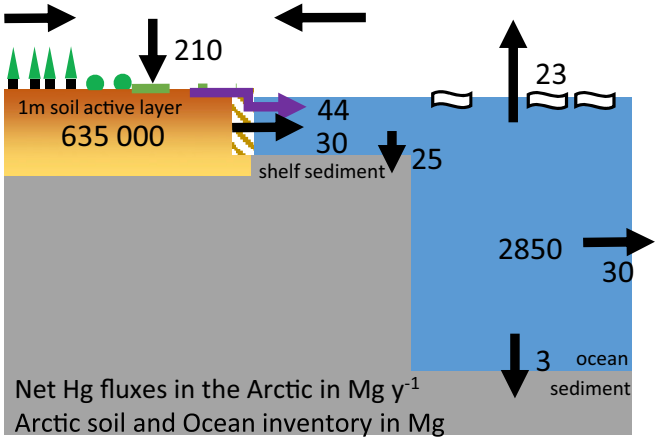

Fig. 7. The modern Arctic Hg cycle, showing net fluxes (Mg y^{-1}) among the different terrestrial, marine, and atmospheric reservoirs from ref. 9. The hatched area represents the coastal erosion Hg flux of 30 Mg y^{-1}. The revised river Hg flux (44 Mg y^{-1}, purple arrow) confirms a new paradigm in which tundra vegetation and soil uptake of atmospheric Hg^0 traffic midlatitude Hg^0 emissions to rivers and the AO. The AO, in turn, exports Hg to the North Atlantic Ocean, the atmosphere, and marine sediments. Recently updated marine (2,850 Mg) and Arctic soil (635,000 Mg) Hg inventories (9, 14, 30) are included to illustrate the potential threat of permafrost thawing on the river Hg flux and AO Hg budget.

permafrost soils (11, 29). The Hg net deposition number includes the active plant Hg^0 uptake of 6.5 $\mu g \cdot m^{-2} \cdot y^{-1}$, the low Hg^{II} wet deposition of 0.5 $\mu g \cdot m^{-2} \cdot y^{-1}$, and the Hg^{II} dry deposition of 2.5 $\mu g \cdot m^{-2} \cdot y^{-1}$ over the 22.79 million square kilometer permafrost soil area (11). The large active-layer soil Hg pool [408 to 863 Gg Hg, mean of 635 Gg (14, 30)] supplies Hg to Arctic rivers and sustains a large spring flood Hg pulse to the coastal AO. Here, river THg (44 Mg y^{-1}), together with coastal erosion Hg inputs (30 Mg y^{-1}), is partially photoreduced in surface waters and emitted to the atmosphere during summertime (8). Midlatitude atmospheric Hg^0 also reaches the AO where wet and dry deposition, especially during springtime AMDE events, is of similar magnitude as terrestrial inputs (76 Mg y^{-1}). However, the large Hg reemissions from ice and AO water (99 Mg y^{-1}) exceed Hg deposition over the AO (Fig. 6*B*). On an annual basis, the AO is therefore a net Hg emission source (23 Mg y^{-1}) to the atmosphere. The AO not only exports Hg to the atmosphere but also to the North Atlantic basin (30 Mg y^{-1}), because marine THg levels in outgoing AO currents, at all depths, are more elevated than in incoming Atlantic waters (21, 31, 32). Lastly, AO Hg is exported to shelf (25 Mg y^{-1}) and deep AO sediments (3 Mg y^{-1}) (9).

The above-outlined AO Hg export scenario for the modern AO has likely changed over the past 50 y. Since 1970, global anthropogenic Hg emissions to air have decreased by a factor of 2 (33). Northern Hemisphere atmospheric Hg deposition to soils has concomitantly decreased by a factor of 2 (34). In the 1980s, Atlantic Ocean surface and intermediate waters had higher Hg concentrations due to enhanced emissions from North America and Europe (31, 35), and AO summer sea-ice extent was larger, possibly inhibiting the strong Hg^0 evasion observed today. Consequently, the AO Hg budget is in constant flux and likely not at steady state, except for the surface ocean, which adapts more rapidly to decadal Hg emission and climate drivers. Future work should investigate (*i*) if and by how much the Arctic river Hg flux will increase as permafrost further thaws, (*ii*) the transport and dynamics of terrestrial Hg in the transpolar drift current, and (*iii*) the Hg export flux from AO surface waters to shelf sediments and deep AO.

ACKNOWLEDGMENTS. We thank Anatoli Pimov for his significant technical help in the field; Laure Laffont and Frederic Candaudap for assistance with laboratory analysis; and Helen Amos, Aiguo Dai, and Anne Soerensen for valuable discussion. DOC analyses were performed at the analytical platform performed at EcoLab by Didier Lambrigot and Frédéric Julien.This work was supported by Grant FP7-IDEAS-ERC 258537 and programme 1207 from the Paul Émile Victor French Polar Institute (to J.E.S.); Grant FP7- PEOPLE-2010-RG 277059 (to R.T.) (www.tomcar.fr); CNRS Chantier Arctique Francais funding via the Pollution in the Arctic System project; CNRS Mission Interdisciplinaire funding via the Changing Siberia project; H2020 Grant 689443 via the Integrative and Comprehensive Understanding on Polar Environments project; and the Groupe de recherche internationaux Carbon, Water and Metal Transport in Wetlands of Siberia and National Polytechnic Institute of Toulouse (INPT) programs. N.T. benefited from INPT support as visiting Professor.

1. Debes F, Weihe P, Grandjean P (2016) Cognitive deficits at age 22 years associated with prenatal exposure to methylmercury. *Cortex* 74:358–369.
2. Roman HA, et al. (2011) Evaluation of the cardiovascular effects of methylmercury exposures: Current evidence supports development of a dose-response function for regulatory benefits analysis. *Environ Health Perspect* 119:607–614.
3. Arctic Monitoring and Assessment Programme (2011) *AMAP Assessment 2011: Mercury in the Arctic* (Arctic Monit Assess Programme, Oslo).
4. Steffen A, et al. (2008) A synthesis of atmospheric mercury depletion event chemistry in the atmosphere and snow. *Atmos Chem Phys* 8:1445–1482.
5. Outridge PM, Macdonald RW, Wang F, Stern GA, Dastoor AP (2008) A mass balance inventory of mercury in the Arctic Ocean. *Environ Chem* 5:1–23.
6. Dastoor AP, Durnford DA (2014) Arctic Ocean: Is it a sink or a source of atmospheric mercury? *Environ Sci Technol* 48:1707–1717.
7. Fisher JA, et al. (2012) Riverine source of Arctic Ocean mercury inferred from atmospheric observations. *Nat Geosci* 5:499–504.
8. Zhang Y, et al. (2015) Biogeochemical drivers of the fate of riverine mercury discharged to the global and Arctic oceans. *Global Biogeochem Cycles* 29:854–864.
9. Soerensen AL, et al. (2016) A mass budget for mercury and methylmercury in the Arctic Ocean. *Global Biogeochem Cycles* 30:560–575.
10. Sonke JE, Heimbürger L-E (2012) Mercury in flux. *Nat Geosci* 5:447–448.
11. Obrist D, et al. (2017) Tundra uptake of atmospheric elemental mercury drives Arctic mercury pollution. *Nature* 547:201–204.
12. Amos HM, et al. (2014) Global biogeochemical implications of mercury discharges from rivers and sediment burial. *Environ Sci Technol* 48:9514–9522.
13. Coquery M, Cossa D, Martin JM (1995) The distribution of dissolved and particulate mercury in three Siberian estuaries and adjacent Arctic coastal waters. *Water Air Soil Pollut* 80:653–664.
14. Schuster PF, et al. (2018) Permafrost stores a globally significant amount of mercury. *Geophys Res Lett* 45:1463–1471.
15. Kirk JL, St Louis VL (2009) Multiyear total and methyl mercury exports from two major sub-Arctic rivers draining into Hudson Bay, Canada. *Environ Sci Technol* 43: 2254–2261.
16. Leitch DR, et al. (2007) The delivery of mercury to the Beaufort Sea of the Arctic Ocean by the Mackenzie River. *Sci Total Environ* 373:178–195.
17. Schuster PF, et al. (2011) Mercury export from the Yukon River Basin and potential response to a changing climate. *Environ Sci Technol* 45:9262–9267.
18. Carrie J, Stern GA, Sanei H, Macdonald RW, Wang F (2012) Determination of mercury biogeochemical fluxes in the remote Mackenzie River Basin, northwest Canada, using speciation of sulfur and organic carbon. *Appl Geochem* 27:815–824.
19. Durnford D, et al. (2012) How relevant is the deposition of mercury onto snowpacks?–Part 2: A modeling study. *Atmos Chem Phys* 12:9251–9274.
20. Kirk JL, et al. (2012) Mercury in Arctic marine ecosystems: Sources, pathways and exposure. *Environ Res* 119:64–87.
21. Heimbürger LE, et al. (2015) Shallow methylmercury production in the marginal sea ice zone of the central Arctic Ocean. *Sci Rep* 5:10318.
22. Raymond PA, et al. (2007) Flux and age of dissolved organic carbon exported to the Arctic Ocean: A carbon isotopic study of the five largest arctic rivers. *Global Biogeochem Cycles* 21:GB4011.
23. Kirk JL, et al. (2008) Methylated mercury species in marine waters of the Canadian high and sub Arctic. *Environ Sci Technol* 42:8367–8373.
24. Dai A, Trenberth KE (2002) Estimates of freshwater discharge from continents: Latitudinal and seasonal variations. *J Hydrometeorol* 3:660–687.
25. Manizza M, et al. (2009) Modeling transport and fate of riverine dissolved organic carbon in the Arctic Ocean. *Global Biogeochem Cycles,* 23:GB4011.
26. Quemerais B, et al. (1999) Sources and fluxes of mercury in the St. Lawrence River. *Environ Sci Technol* 33:840–849.
27. Lammers RB, Shiklomanov AI, Vorosmarty CJ, Fekete BM, Peterson BJ (2001) Assessment of contemporary Arctic river runoff based on observational discharge records. *J Geophys Res D Atmos* 106:3321–3334.
28. McClelland J, Dery S, Peterson B, Holmes R, Wood E (2006) A pan-arctic evaluation of changes in river discharge during the latter half of the 20th century. *Geophys Res Lett* 33:L06715.
29. Jiskra M, et al. (2018) A vegetation control on seasonal variations in global atmospheric mercury concentrations. *Nat Geosci* 11:244–250.
30. Olson C, Jiskra M, Biester H, Chow J, Obrist D (2018) Mercury in active-layer tundra soils of Alaska: Concentrations, pools, origins, and spatial distribution. *Global Biogeochem Cycles* 32:1058–1073.
31. Cossa D, et al. (2018) Sources, cycling and transfer of mercury in the Labrador Sea (GEOTRACES-GEOVIDE cruise). *Mar Chem* 198:64–69.
32. Cossa D, et al. (2018) Mercury distribution and transport in the North Atlantic Ocean along the GEOTRACES-GA01 transect. *Biogeosciences* 15:2309–2323.
33. Horowitz HM, Jacob DJ, Amos HM, Streets DG, Sunderland EM (2014) Historical mercury releases from commercial products: Global environmental implications. *Environ Sci Technol* 48:10242–10250.
34. Amos HM, et al. (2015) Observational and modeling constraints on global anthropogenic enrichment of mercury. *Environ Sci Technol* 49:4036–4047.
35. Soerensen AL, et al. (2012) Multi-decadal decline of mercury in the North Atlantic atmosphere explained by changing subsurface seawater concentrations. *Geophys Res Lett* 39:L21810.
36. Mann PJ, et al. (2016) Pan-Arctic trends in terrestrial dissolved organic matter from optical measurements. *Front Earth Sci,* 4:25.